A. Simon Justin, P. Vickraman* and B. Joji Reddy

Investigation on Carbonsphere@Nickel Cobalt Sulfide Core-shell Nanocomposite for Asymmetric Supercapacitor Application

https://doi.org/10.1515/ehs-2019-0003

Abstract: The carbon sphere (CS)@nickel cobalt sulfide core-shell nanocomposite at five different mole ratios have been synthesized by a facile low-temperature water-bath method without any thermal treatment. The XRD results on CS, $NiCo_2S_4$ and its ternary complexation confirms nanocomposite formation which matches with the cubic structure. The FTIR confirms the complexation of CS and metal-sulfide core-shell. TEM morphology shows CS at $NiCo_2S_4$ forming a core-shell which appears as interlinked bunch of grapes. The BET surface analysis observes the high surface area for the core-shell. The XPS studies confirm the elemental presence and valence states of metal composition of the core-shell. Electrochemical studies on the pure $NiCo_2S_4$ and CS@$NiCo_2S_4$ have shown that CS@$NiCo_2S_4$ in 1:1 ratio (scn2) only exhibits higher specific capacitance of 838 F g^{-1} at 1 A g^{-1} with capacity retention of 89 % for 5000 cycles than other mole ratios. Using this scn2, asymmetric supercapacitor (ASC) device fabrication has been studied. The electrochemical studies on ASC reveal high energy density of 101 Wh kg^{-1} with the power density of 6.3 k W kg^{-1}, and having good cycling stability with 92% of capacitance retention even after 3000 cycles at 20 A g^{-1}.

Keywords: low temperature water-bath, core-shell, mesoporous, nanocomposite, asymmetric supercapacitor

Introduction

Consumer electronics and modern electronic gadgets have become the order of the day for every common man. Cellular phone, laptop, can-camera, and household electronic goods are having tough competition in the consumer market. Each passing day, with new options and features, the market is flooded with newer devices and gadgets. These modern-day gadgets rely heavily on energy storage and delivery parameters. In this context, supercapacitors have revolutionized and in certain cases replaced the batteries for some electrochemical applications due to their good power density and quick charging/deliverance of power (watts = voltage times the current) so enormous interest and extensive attention has been given to supercapacitors by the researchers for the past two decades (Zhai et al. 2011; Jiang et al. 2012; Wang, Zhang, and Zhang 2012; Wu and Zhang 2017).

A variety of electrodes are investigated based on carbonaceous (Manaf, Bistamam, and Azam 2013; Hao, Li, and Zhi 2013), transition metal oxides (Snook, Kao, and Best 2011; Nguyen et al. 2015; Wei et al. 2018c), conducting polymers (Lokhande, Dubal, and Joo 2011; Lamiel, Kumar, and Shim 2017) and so on, however they have their drawbacks, i. e. carbon materials have lower specific capacitance, low electrical conductivity for transition metal oxides and very poor cyclability of conducting polymer (Yuan et al. 2014; Chen and Dai 2013; Shown et al. 2014; Wang et al. 2016). On the other hand, the transition metal sulfides exhibit good reversibility, cyclability and high theoretical capacitance (Pu et al. 2014; Lin, Tai, and Chou 2014; Yang, Chen, and Chang 2011; Chou and Lin 2013; Zhu et al. 2011; Hou et al. 2011; Wei et al. 2018a; Cheng et al. 2017). Amongst sulfides, the ternary metal sulfides ($NiCo_2S_4$) have attracted a lot of attention as electrodes for supercapacitors owing to their excellent electrochemical performance (Yang et al. 2016; Nguyen, Lamiel, and Shim 2015; Chen et al. 2013; Xiao et al. 2014; Hu et al. 2009; Zou et al. 2016). Albeit this appealing performance, ternary metal sulfides have shown low rate performance at higher current density and lower cycling stability (Beka, Li, and Liu 2017).

The researchers have carefully attempted to avoid the inherent low rate performance of $NiCo_2S_4$ by increasing the active surface area by synthesizing it in nano core-

***Corresponding author: P. Vickraman,** Solid State Ionics Lab, Department of Physics, Gandhigram Rural Institute Deemed University, Gandhigram, Tamil nadu 624302, India,
E-mail: vrsvickraman@yahoo.com
https://orcid.org/0000-0002-5200-4682
A. Simon Justin: E-mail: simjus6@gmail.com, **B. Joji Reddy,** Solid State Ionics Lab, Department of Physics, Gandhigram Rural Institute Deemed University, Gandhigram, Tamil nadu 624302, India

shell structures. The core-shell structure of $NiCo_2S_4$ has improved the low rate performance and cycling stability but is not stable (Beka, Li, and Liu 2017). So in order to improve stability on the rate performance and cycling stability $NiCo_2S_4$ is hybridized with carbon material (Lamiel et al. 2016; Justin, Vickraman, and Reddy 2018). The researchers found that Carbon in spherical symmetry (CS) with $NiCo_2S_4$ provides high surface area, excellent conductivity, and good mechanical as well as chemical stability for supercapacitors (Justin, Vickraman, and Reddy 2018). Based on the review of CS as a core templating with $NiCo_2S_4$ as a shell for the successful accomplishment of electrochemical performance the present study is focused on CS@$NiCo_2S_4$ core-shell composite. The synthesis and performance study of CS@$NiCo_2S_4$ had been carried out by Lamiel et al. via hydrothermal method and reported the specific capacitance of 724 F g^{-1} at 2 A g^{-1} with 86.1 % capacity retention for 2000 charge/discharge cycles using nickel foam as a substrate (Lamiel et al. 2016). But in this work, the investigation is based on synthesis of CS@$NiCo_2S_4$ via low temperature water-bath method and the performance will be discussed on the synthesizing route (Justin, Vickraman, and Reddy 2018).

Experimental

Materials

The $Ni(OCOCH_3)_2{\cdot}4H_2O$ (98 %), $Co(OCOCH_3)_2{\cdot}4H_2O$ (98 %), Ethanol (96 %), Glucose (99 %) and Acetylene Black (98 %) were purchased from Alfa Aesar UK, and used without any further purification. The Polytetrafluoroethylene 60 % emulation (PTFE) and Thiourea (CH_4N_2S, 99 %) were obtained from Sigma Aldrich (U.S.A) and used as such.

Synthesis of Carbon Sphere

Synthesis of Carbon sphere (CS) was carried out using hydrothermal method wherein 0.5 molar aqueous homogeneous glucose solutions was obtained by mechanical stirring. This as-prepared homogeneous solution was poured onto a Teflon-lined container and placed in an appropriate autoclave at 180 °C for initiating hydrothermal reaction to take place within the time module of 10 hrs. The final resultant product was obtained from autoclave at room temperature, and subsequently centrifuged and constantly washed with double distilled water and thereafter three times with ethanol. Evantually, the brownish CS powder collected was dried at 60 °C overnight for further use.

Syntheses of Core-shell Carbonsphere@Nickel Cobalt Sulfide Nanocomposites

The synthesis core-shell carbonsphere@nickel cobalt sulfide nanocomposites (CS@$NiCo_2S_4$) was done by adopting a simple low temperature water-bath technique (Justin, Vickraman, and Reddy 2018). The precursors namely nickel acetate tetrahydrate ($Ni(OCOCH_3)_2{\cdot}4H_2O$) and cobalt acetate tetrahydrate ($Co(OCOCH_3)_2{\cdot}4H_2O$), respectively of 1.25 g and 2.5 g were thoroughly dissoluted in 50 mL ethanol and stirred for getting homogeneous solution. Further as prepared CS, in Section 2.2, in 0, 0.5, 1.0, 1.5 and 2.0 mole ratios was dissolved in 30 mL of ethanol for the constant content of 1 molar nickel cobalt sulfide i. e. [CS:$NiCo_2S_4$ = 0:1(scn0), 0.5:1(scn1), 1:1(scn2), 1.5:1(scn3) and 2:1(scn4)] and mechanically agitated for getting complete dissolution of the solution. The mixture of nickel acetate and cobalt acetate solution was kept in a constant temperature (60 °C) water-bath. The CS solution was dripped as drops into the mixed solution of nickel/cobalt acetate and continuously stirred for an hour to have complete dissolution. The aqueous 0.6 M thiourea (CH_4N_2S) was prepared with 50 mL of double distilled water, and this solution was added drop wise into the mixed solution which was subsequently maintained at constant temperature (60 °C) water bath for 2 hrs with continuous stirring. The end product as obtained was thoroughly rinsed three times with distilled water as well as ethanol, and dried overnight at 60 °C. Thus the way of core-shell CS@$NiCo_2S_4$ nanocomposites were synthesized.

Characterization

The XRD of the as-prepared materials was examined using XPERT-PRO diffractometer of Cu-Kα radiation of λ = 1.5406 Å in 30 mA/40 kV between 10 ° to 80 °. The FT-IR of the samples was traced using JASCO 640 plus infrared spectrometer in the range of 4000–400 cm^{-1}. The TEM images were recorded using JEOL JEM-2100 with the resolution 0.23 nm. The BET surface areas were measured by nitrogen adsorption/desorption method using a NOVA2200e gas sorption analyzer (Quantachrome Corp. USA). The elemental composition and electronic configuration were analyzed by X-ray

photoelectron spectroscopy (XPS, Thermo Scientific, K-Alpha) using monochromatized Al-Kα radiation.

Electrochemical Studies

The pristine nickel cobalt sulfide ($NiCo_2S_4$) and composite ($CS@NiCo_2S_4$) were used as active materials with conductive acetylene black and Polytetrafluoroethylene for preparing the slurry in the weight ratio 85:10:5 respectively in a ethanol solvating medium. This as -obtained slurry was spread onto the graphite sheet substrate and dried over the hot plate at 60 °C for about 10 hrs for getting electrodes. The electrodes were subjected to electrochemical studies to understand the electrochemical performance in three-electrode set up (a platinum foil as a counter, Ag/AgCl as a reference and the active material as a working electrode (mass = 1 mg; area = 1 cm^2)); in 3 M KOH aqueous solution as a electrolyte using CHI 660D electrochemical workstation (ChenHua Instruments, Shanghai) at room temperature. Further, asymmetric supercapacitor was fabricated using $CS@NiCo_2S_4//rGO$ and its electrochemical performance was also studied. The specific capacitances of the $NiCo_2S_4$ and core-shell composites were calculated by the following equation.

$$C = \frac{I \times \Delta t}{m \times \Delta V} \text{ F g}^{-1} \quad (1)$$

The mass balance is calculated using

$$\frac{m^+}{m^-} = \frac{C^- \times V^-}{C^+ \times V^+} \quad (2)$$

The coulombic efficiency was calculated using

$$\eta = \frac{t_d}{t_c} \times 100\,\% \quad (3)$$

The energy and power density were by

$$E = \frac{1}{2} CV^2 \text{ Wh kg}^{-1} \quad (4)$$

$$P = \frac{E}{\Delta t} \times 3600 \text{ W kg}^{-1} \quad (5)$$

where 'C' is the specific capacitance, 'I' is the current, 'm' is the mass of active materials, 'Δt' is the discharge time, 'ΔV' is the discharge voltage, 'm^+' – mass of the positive electrode, m^- – mass of the negative electrode, C^-, V^-, C^+, V^+ are the capacitance and the potential window of the positive and negative electrode, 'η' – the columbic efficiency, 't_d' – the discharge time, 't_c' – the charging time, 'E' is the energy density, 'V' potential window and 'P' is the power density.

Result and Discussion

The XRD studies on as-prepared pristine CS, pristine $NiCo_2S_4$ and the ternary composite CS@ $NiCo_2S_4$ are carried out (Figure 1). In Figure 1(a), peak at $2\theta = 20°$ corresponds to carbon sphere which confirms the carbonization of the glucose (Justin, Vickraman, and Reddy 2018). The Figure 1(b) shows the characteristics peaks of the pristine nano $NiCo_2S_4$ (scn0) appeared at 20° (111), 33.7° (220) and 60° (422) which match with JCPDS- 20–0782 of cubic structure. Even though the cobalt stoichiometry molar ratio is high in $NiCo_2S_4$, there is no trace of it in the composites. This may be due to the cobalt occupation in the nickel sites (possibly because of same ionic sizes) are not altered the structure (Mi et al. 2015). The Figure 1(c) shows the XRD pattern of $CS@NiCo_2S_4$ composite (scn1). The peak at $2\theta = 20°$ in both CS and $NiCo_2S_4$ are merged and appeared as broadened hump, and no changes are observed in the peaks of scn0 at 33.7° and 60° in scn1. Further, increasing the amount of nano CS, the peak at 20° is highly broadened

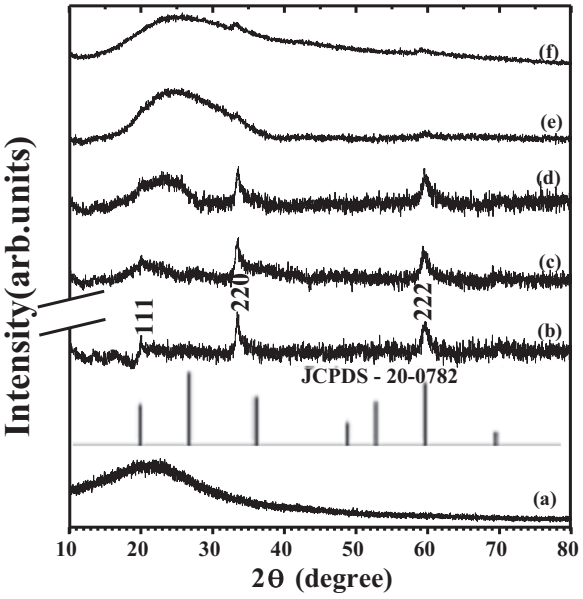

Figure 1: XRD diffractogram of (a) CS, (b) scn0, (c) scn1, (d) scn 2, (e) scn 3 and (f) scn 4.

in scn2, scn3 and scn4 (Figure 1(d–f)), and also no change of position of other peaks are noted. Thus XRD studies has revealed that the nano composites with CS are in amorphousness which in turn has facilitated for improving the electrode/electrolyte interface causing better electrochemical performance (Beka, Li, and Liu 2017; Lamiel et al. 2016; Justin, Vickraman, and Reddy 2018).

FTIR spectra of the as-prepared materials are recorded to understand complexation of various constituents (Figure 2). The spectra show the vibration bands at 493 and 617 cm^{-1} respectively represent the metal (Ni-Co) and sulfide (S) stretching's (Zheng et al. 2018). This confirmed the molecular complexation of $NiCo_2S_4$. The vibration peak at 1024 cm^{-1} indicates the C-O stretching mode. The stretching vibrational modes at 1698 cm^{-1} and 1551 cm^{-1} correspond to O-H group. The peak at 1375 cm^{-1} confirms the presence of CO_3^{-2} ions (Wu et al. 2004). While increasing the concentration of CS, the peak at 617 cm^{-1} has been broadened which suggests the complexation of CS and $NiCo_2S_4$.

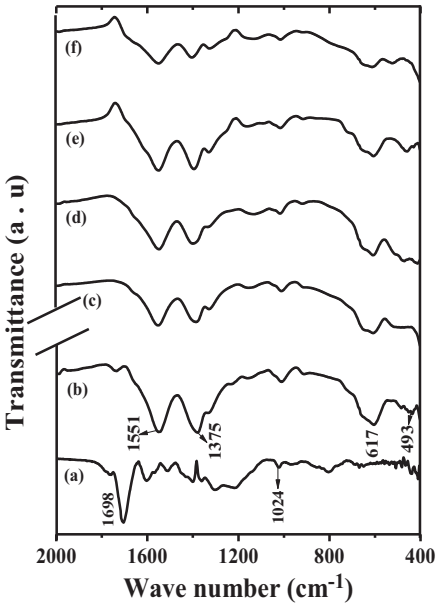

Figure 2: FTIR spectra of (a) CS, (b) scn0, (c) scn1, (d) scn 2, (e) scn 3 and (f) scn 4.

The specific surface area and pore size distribution of pure $NiCo_2S_4$ and CS@$NiCo_2S_4$ are observed through N_2 adsorption/desorption isotherms, as shown in Figure 3. The type-IV H3 hysteresis loop is attributed to both pure (Figure 3(a)) and composite (Figure 3(b)) which are confirming the mesoporous structure (Thommes et al. 2015). The high surface area of 53.5 m^2 g^{-1} is observed for scn2 compared to 42.8 m^2 g^{-1} of scn0. The inset fig. gives the pore calculation of scn2 and scn0 using Barret-Joyner-Halenda (BJH) method. The pore size of mesoporous structure of scn2 is 7.15 nm whereas for scn0 it is 2.78 nm. The higher pore size seems to be good enough for electrolyte penetration unto act as a reservoir (Mohamed, Attia, and Hassan 2017) for creating sufficient path ways for ion transport and resulting in enhanced of the pseudocapacitive performance of scn2 (Justin, Vickraman, and Reddy 2018) in the present study.

The electronic state and elemental composition of CS@$NiCo_2S_4$ core-shell are examined by XPS. The Figure 4(a) shows the Ni 2p photoelectron spectrum. The doublet peaks of Ni $2p_{3/2}$ and Ni $2p_{1/2}$ are noted at 860 eV and 879 eV respectively. The peaks at 853 and 870 eV represent the Ni^{2+} and 855 and 873 eV are attributed to Ni^{3+}. These intense satellite peaks indicate that the main valence state of nickel is at Ni^{2+} (Wen et al. 2017). The Figure 4(b) shows two peaks which are ascribed to Co $2p_{3/2}$ and Co $2p_{1/2}$ having two

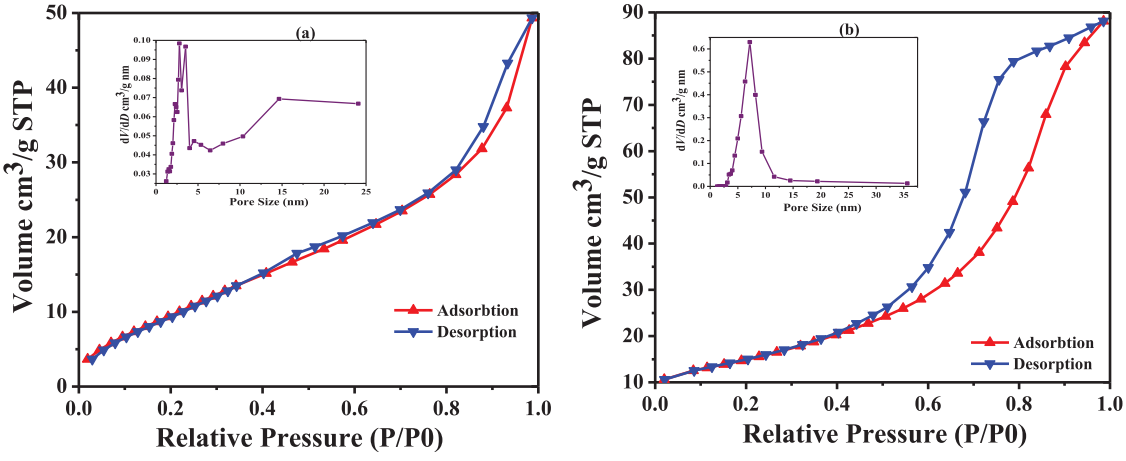

Figure 3: XPS analysis of nco3 nanocomposite sphere (a) Ni 2p, (b) Co 2p, (c) S 2p and (d) C 1s.

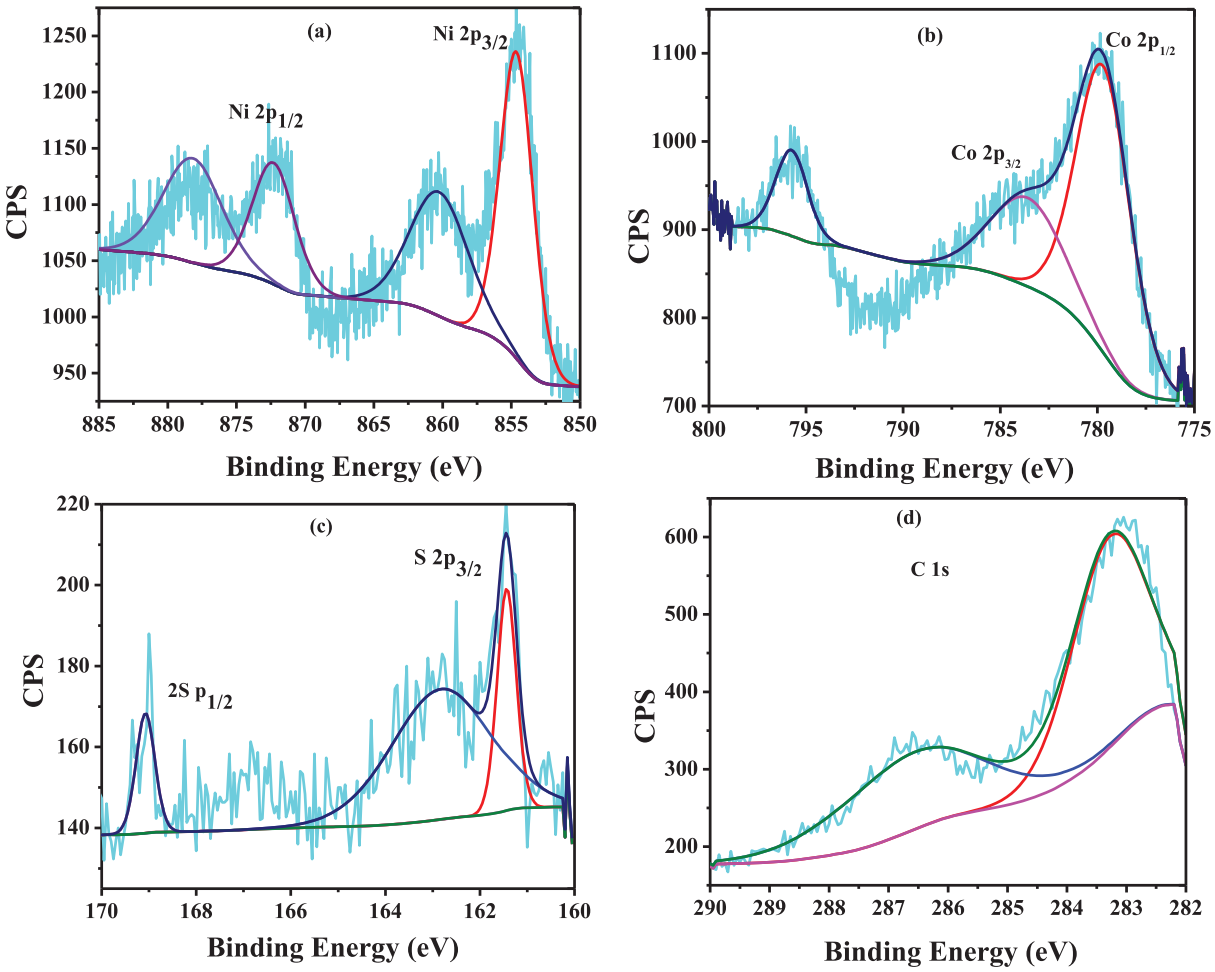

Figure 4: BET surface and pore size studies of (a) scn0 and (b) scn 2.

satellite peaks at 783 eV and 802 eV. These indicate that the most of Co ion are present in the Co^{3+} state (Chen et al. 2017). The deconvoluted peaks at 778 eV and 793 eV correspond to Co^{3+} (Chen et al. 2017) and peaks at 780 eV and 796 eV are assigned to Co^{2+} (Chen et al. 2017). In Figure 4(c), the S 2p spectrum is fitted with one main peak and one satellite peak. The peak at 161 eV corresponds to S $2p_{3/2}$ and at 162.5 eV assigned to metal – sulfur bond which corresponds to S $2p_{1/2}$ reveals the existence of sulfur ions in low coordination onto the surface. The peak at 169 eV is attributed to the surface-adsorbed oxidized sulfur species (SO_4^{2-} and HSO^{4-}) (Khani and Wipf 2017). The Figure 4(d) shows C 1s spectrum wherein the peak at 284.6 eV corresponds to sp2 hybridized carbon and the peak at 285.6 eV is ascribed to C-heteroatom bond and a peak at 288 eV is assigned to O-C = O group (Meng et al. 2017).

The TEM morphology of as-prepared pristine nano CS, nano $NiCo_2S_4$ and CS@$NiCo_2S_4$ are shown in Figure 5. In Figure 5(a), CS appears as a perfect shape of spheres in a bunch with smooth surface in different sizes. The Figure 5(b) image of pristine nano $NiCo_2S_4$ appears as a scattered nano flake with sponge like surface but CS@$NiCo_2S_4$ (scn2) nanocomposite core-shell (Figure 5(c)) looks like an interlinked bunch of grapes. The composite surface morphology clearly confirms the core-shell formation. The cause for the formation is due to the presence of carboxyl and hydroxyl groups (Justin, Vickraman, and Reddy 2018) of carbon sphere's strong orientation with the metal sulfides which might be the reason for the formation of the stable core-shell. In other words, this stable core-shell configuration favors to entrap the electrolyte into the bulk of the electrode material and improving the electrode/electrolyte interaction which inturn leads to causing for better electrochemical performance (Lamiel et al. 2016). The Figure 5(d) shows existence of scn2 core-shell in the amorphous phase. Figure 5(e) represents the EDAX spectrum of core-shell nano composite.

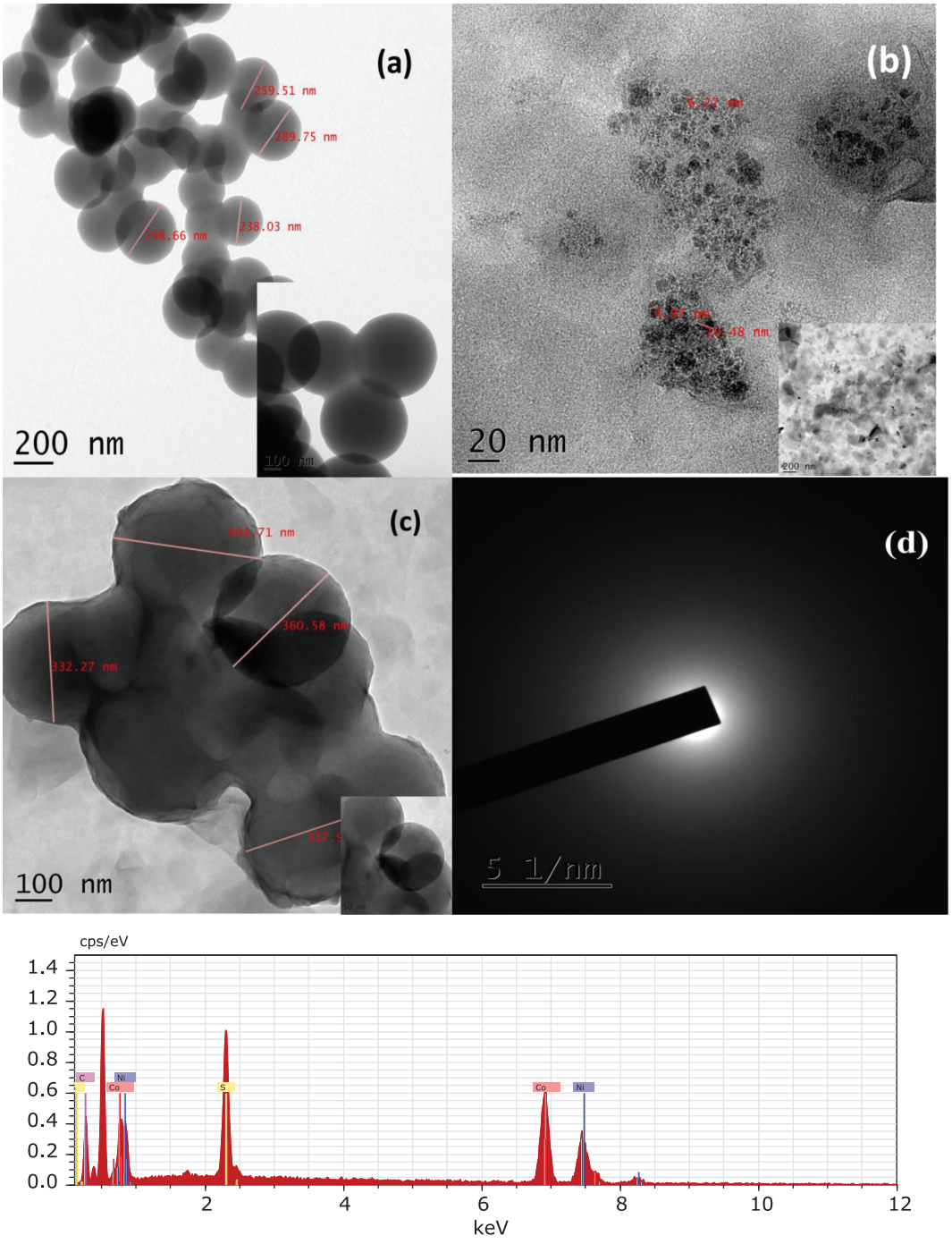

Figure 5: TEM morphological studies of (a) CS, (b) scn0 (c) scn2 and (d) SAED pattern of scn2 (e) EDS mapping of scn2.

The electrochemical studies of nano $NiCo_2S_4$ and nano core-shell composites CS@$NiCo_2S_4$ carried out in three electrode mode in 3 M KOH electrolyte. The cyclic voltametry (CV) study is carried at different scan rates (2 mVs^{-1}–100 mVs^{-1}) in potential window −0.1 V – 0.5 V. Irrespective of varying load of CS, a pair of redox process is noted in all electrode materials (Figure 6(a–e)), corresponding to the redox process of Co^{2+} /Co^{3+} /Co^{4+} and Ni^{2+} /Ni^{3+} (Peng et al. 2016).

$$NiCo_2S_4 + OH^- + H_2O \Leftrightarrow NiSOH + 2CoSOH + e^- \quad (6)$$

$$CoSOH + OH^- \Leftrightarrow CoSO + H_2O + e^- \quad (7)$$

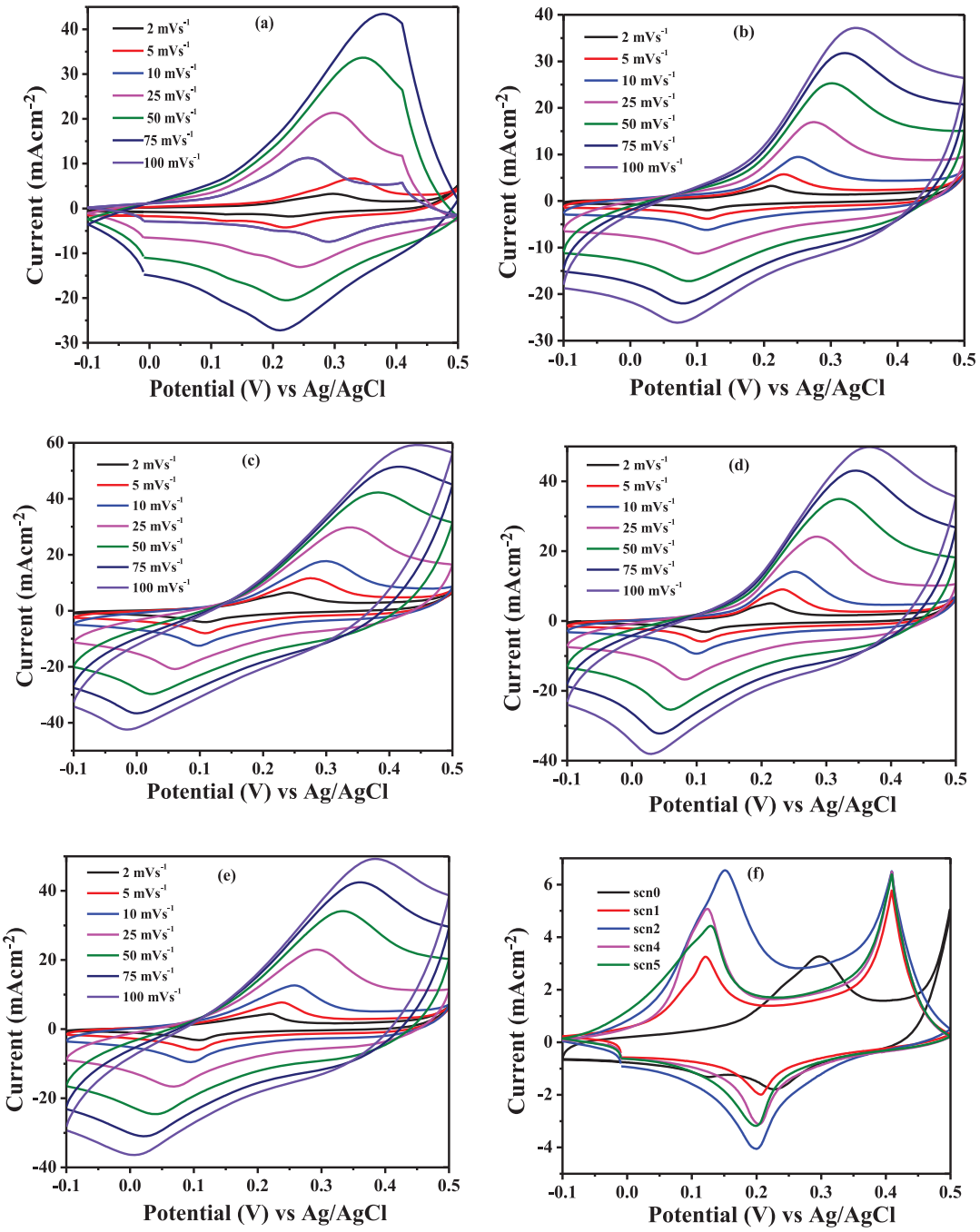

Figure 6: Cyclic Voltagram of (a) scn0, (b) scn1, (c) scn2, (d) scn3, (e) scn4 and (f) Comparison of CV curve at 2 mVs^{-1}.

It is observed that the shifting of oxidation peak at higher potential and as that of reduction peak at lower potential is noted by increasing the scan rate. This is because the diffusion rate of electrolyte is not sufficient for fulfilling the electrochemical reaction of active material (Peng et al. 2016; Chen et al. 2017; Wei et al. 2018b; Zhi et al. 2013). The Figure 6(f) presents the CV curves of all CS@$NiCo_2S_4$ electrode materials in scan rate of 2 mVs^{-1}, and it is found that the scn2 core-shell nanocomposite has larger area under CV curve which has provided high electrochemical performance.

The galvanostatic charge/discharge studies are carried out for both pristine $NiCo_2S_4$ as well as all CS@$NiCo_2S_4$ composite in −0.2 V – 0.4 V potential difference for different current densities of 1, 2, 5, 10 and 20 A g^{-1} (Figure 7). The discharge curves clearly indicate that pesudocapacitance

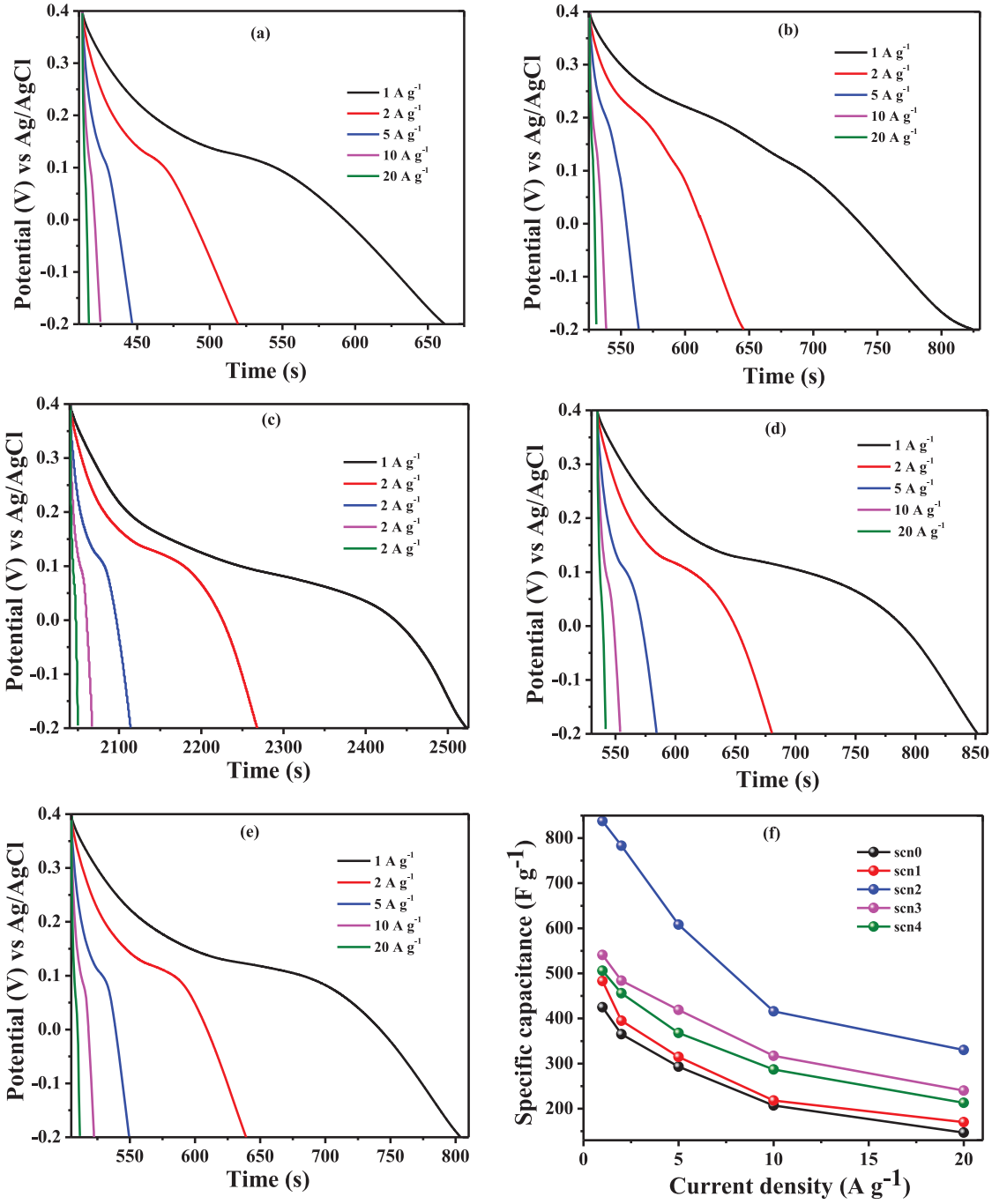

Figure 7: Galvanostatic charge/discharge studies of (a) scn0, (b) scn1, (c) scn2, (d) scn3, (e) scn4 and (f) Specific capacitance of GCD curve at different current densities.

behavior of them. In other words, the two segment of discharge curve are observed i.e, internal resistance and change in energy within the capacitor (Xiao et al. 2014). The specific capacitances are calculated using the equation and is found to be 425, 365, 293, 207 and 147 F g^{-1} for scn0 (Figure 7(a)); 483, 395, 315, 218 and 170 F g^{-1} for scn1 (Figure 7(b)); 838, 783, 608, 416 and 330 F g^{-1} for scn2 (Figure 7(c)); 541, 484, 419, 317 and 240 F g^{-1} for scn3 (Figure 7(d)); and for scn4 (Figure 7(e)), 506, 456, 368, 287 and 213 F g^{-1} at current densities mentioned earlier. The comparisons of calculated specific capacitance of all the electrode materials are depicted in Figure 7(f). Amongst the electrodes, scn2 has showed higher specific capacitance and rate capability than other electrodes, i. e. TEM morphology core-shell mesoporous structure favors for

acting as a electrolyte reservoir not only the surface but also on the bulk of the material (Beka, Li, and Liu 2017; Cherusseri and Kar 2015). This internal reservoir is bringing the internal active surface layers directly in contact with electrolyte, facilitating for the enhancement of diffusivity rate of ion for fast ion transportation leading to better redox reactions to take place (Wang et al. 2012). The concentration dependency of CS is reflecting on the deterioration of the electrochemical performance is noted i. e. increasing thickness raises the inability of ion transfer in the electrode/electrolyte contact surface and as a result higher internal resistance and shorter charge/discharge cycle (Nguyen, Lamiel, and Shim 2015).

The electrochemical impedance studies (EIS) of as-prepared materials are carried out for understanding the favorable kinetics and rapid ion transport in the frequency range 0.01 Hz – 1 MHz. The impedance spectra are fitted with an equivalent series circuit which contain the bulk solution resistance, (R_s) charge–transfer resistance (R_{ct}), the double layer capacitance (C_{dl}), the pseudocapacitance (C_{ps}), and the Warburg impedance (W) (inset in Figure 8(a)). The analysis of EIS is related to equivalent series resistance (R_{ESR}), semi–circle at high frequency and slope at low frequency. The low R_{ESR} is observed for the core-shell scn2 (Table 1).The semi-circle in the high frequency region corresponds to low charge transfer resistance (Table 1) of core-shell nanocomposites CS@$NiCo_2S_4$ (scn2) (Figure 8(a)) for enhancing the ion transport (Sun et al. 2017). In other words CS increment at $NiCo_2S_4$ the scn2 core-shell has showed the better diffusion is observed.

The cycling stability of scn2 core-shell composite has been carried out in a constant current density 20 A g^{-1} for 5000 charge/discharge cycles (Figure 8(b)). It is noted that the good capacity retention of 89 % and 95 % coulombic efficiency for 5000 cycles (equation). The core-shell structure showed the good cycling performance. The main attributing factor of core-shell composition is that the core template CS is fully covered by the nano flake $NiCo_2S_4$ shell, which directly interacts with the electrolyte improving the mechanical stability and good electrical conductivity (Beka, Li, and Liu 2017).

Table 1: Impedance data of the electroactive materials.

Sample code	Solution Resistance (R_s) ohm	Charge Transfer Resistance (R_{ct}) ohm
scn0	0.814	1.353
scn1	0.669	0.829
scn2	0.780	0.19
scn3	1.137	1.107
scn4	1.122	1.040

The electrochemical performance of as-prepared rGO has been examined in three electrode system for device fabrication (Ag/AgCl as a reference electrode; platinum wire as a counter electrode and rGO as a working electrode with the aqueous 3 M KOH as a electrolyte). The Figure 9(a) shows the CV performance of rGO in a rectangular shape which confirms the behavior of it as a double layer capacitor. The ramp shapes (Figure 9(b)) of the GCD curves have also confirmed the double layer capacitative behavior. The specific capacitance is calculated (eq. (1)) and is given as 370 F g^{-1} at 3 A g^{-1}.

To examine the practical application of the core-shell nanocomposite CS@$NiCo_2S_4$ (scn2) the asymmetric supercapacitor (ASC) cell (CS@$NiCo_2S_4$//rGO) is fabricated wherein scn2 as a positive electrode, reduced graphene oxide (rGO- laboratory prepared) as a negative electrode

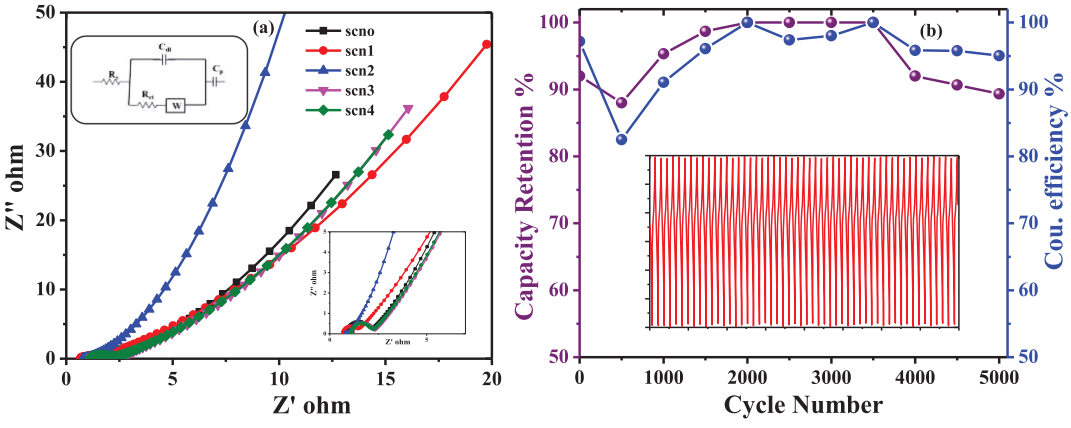

Figure 8: (a) Electrochemical impedance spectrum of the electrodes with fitting circuit and (b) Capacity retention and Coulombic efficiency of scn2.

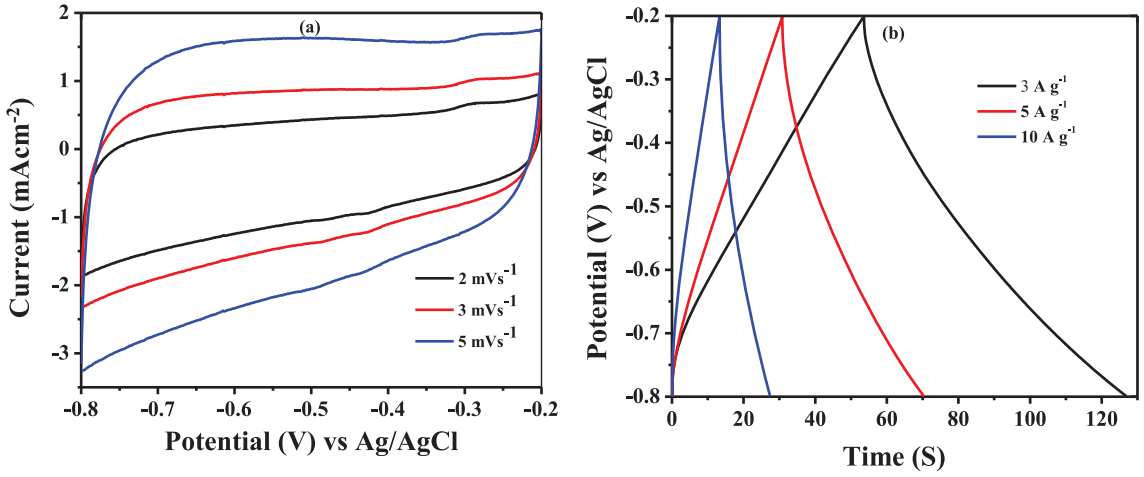

Figure 9: Electrochemical performance of rGO (a). CV curve (b). GCD curve.

and 6 M KOH as a electrolyte were used. The Figure 10 shows the electrochemical performance of the asymmetric capacitor. The Figure 10(a) depicts the CV curves of ASC over the potential window 0–1.4 V at the scan rate from 10 mVs^{-1} – 200 mVs^{-1}. This is exhibiting redox peaks at all scan rates indicating the faradic process. The Figure 10(b)

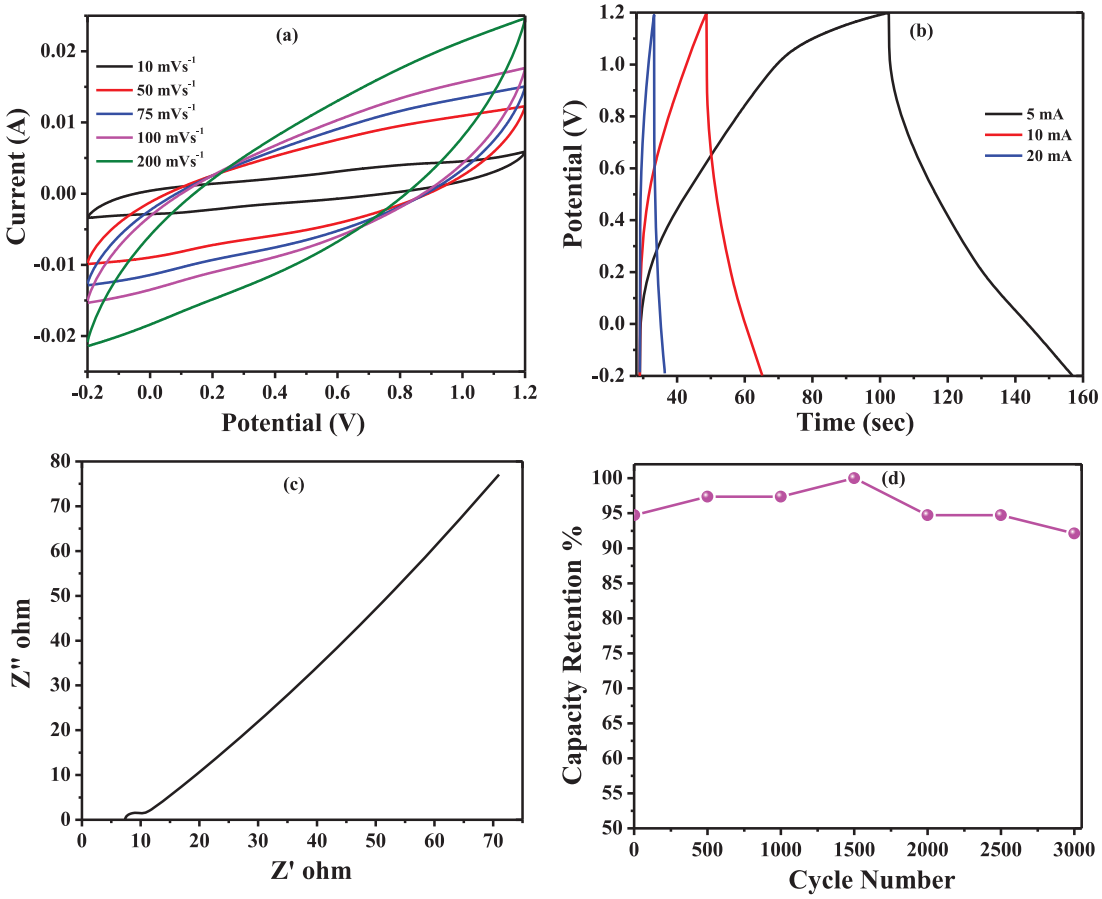

Figure 10: Electrochemical performance of scn2 // rGO asymmetric supercapacitor device (a) CV curves, (b) Charge/discharge profile (c) Impedance spectrum and (d) Capacity retention.

shows the GCD behavior of the ASC at the current densities of 5, 10 and 20 A g^{-1}. The non-linear shape of the charge/discharge profile has revealed the faradic type performance of ASC. The specific capacitances 103, 62.5 and 23.5 F g^{-1} at current densities 5, 10 and 20 A g^{-1} respectively are calculated using equation. The mass is calculated using the equation. The cycling stability of ASC is observed through the continuous charge/discharge cycle at constant current density of 20 A g^{-1} with 92% capacity retention for 3000 cycles (Figure 10(c)) is noted and indicates the good reversibility and stability of ASC. The energy and power densities are calculated 101 Wh kg^{-1} and 6.3 k W kg^{-1} respectively. These observed energy and power densities are quite high with reference to the recently reported $NiCo_2S_4$ (Wang et al. 2012; Li et al. 2014; Chen, Xia, and Alshareef 2014; Hu et al. 2014; Huang et al. 2016; Yan et al. 2016; Chen et al. 2014) based asymmetric capacitors.

Conclusions

The pure $NiCo_2S_4$ and interlinked mesoporous core-shell nanocomposite CS@$NiCo_2S_4$ have successfully been prepared via low temperature water-bath method without any further physical and chemical treatment and confirmed by TEM studies. The XRD diffractogram reveals the cubic structure of the as-prepared materials. The surface area and the mesoporous network of the interlinked core-shell are examined by BET analysis. The XPS analysis suggests the elemental presence and the oxidation states of the element in the core-shell nanocomposite. The TEM morphological study confirms the interlinked core-shell structure. The electrochemical studies report that CS@$NiCo_2S_4$ (scn2, 1:1) composite exhibits the higher specific capacitance (838 F g^{-1} at 1 A g^{-1}) with 89% of capacity retention and 95% of coulombic efficiency for 5000 cycles. The asymmetric supercapacitor CS@$NiCo_2S_4$//rGO has been fabricated and it shows the energy density of 101Wh kg^{-1} and power density of 6.3 kW kg^{-1} and the capacity retention of 92% sustained for 3000 cycles at 20 A g^{-1}.

References

Beka, L. G., X. Li, and W. Liu. 2017. "Nickel Cobalt Sulfide Core/Shell Structure on 3D Graphene for Supercapacitor Application." *Scientific Reports* 7: 2105.

Chen, H., J. Jiang, L. Zhang, H. Wan, T. Qi, and D. Xia. 2013. "Highly Conductive $NiCo_2S_4$ Urchin-like Nanostructures for High-Rate Pseudocapacitors." *Nanoscale* 5: 8879.

Chen, H., J. Jiang, L. Zhang, D. Xia, Y. Zhao, D. Guo, T. Qi, and H. Wan. 2014. "*In Situ* Growth of $NiCo_2S_4$ Nanotube Arrays on Ni Foam for Supercapacitors: Maximizing Utilization Efficiency at High Mass Loading to Achieve Ultrahigh Areal Pseudocapacitance." *Journal of Power Sources* 254: 249.

Chen, T., and L. Dai. 2013. "Carbon Nanomaterials for High-Performance Supercapacitors." *Materials Today* 16: 272.

Chen, W., C. Xia, and H. N. Alshareef. 2014. "One-Step Electrodeposited Nickel Cobalt Sulfide Nanosheet Arrays for High-Performance Asymmetric Supercapacitors." *ACS Nano* 8: 9531.

Chen, X., D. Chen, X. Guo, R. Wang, and H. Zhang. 2017. "Facile Growth of Caterpillar-like $NiCo_2S_4$ Nanocrystal Arrays on Nickle Foam for High-Performance Supercapacitors." *ACS Applied Materials & Interfaces* 9: 18774.

Cheng, C., D. Kong, C. Wei, W. Du, J. Zhao, Y. Feng, and Q. Duan. 2017. "Self-template Synthesis of Hollow Ellipsoids Ni-Mn Sulfides for Supercapacitors, Electrocatalytic Oxidation of Glucose and Water Treatment." *Dalton Transactions* 46: 5406.

Cherusseri, J., and K. K. Kar. 2015. "Hierarchically Mesoporous Carbon Nanopetal Based Electrodes for Flexible Supercapacitors with Super-long Cyclic Stability." *Journal of Materials Chemistry A* 3: 21586.

Chou, S. W., and J. Y. Lin. 2013. "Cathodic Deposition of Flaky Nickel Sulfide Nanostructure as an Electroactive Material for High-Performance Supercapacitors." *Journal of the Electrochemical Society* 160: D178.

Hao, L., X. Li, and L. Zhi. 2013. "Carbonaceous Electrode Materials for Supercapacitors." *Advanced Materials* 25: 3899.

Hou, L., C. Yuan, D. Li, L. Yang, L. Shen, F. Zhang, and X. Zhang. 2011. "Electrochemically Induced Transformation of NiS Nanoparticles into $Ni(OH)_2$ in KOH Aqueous Solution Toward Electrochemical Capacitors." *Electrochimica Acta* 56: 7454.

Hu, L., J. W. Choi, Y. Yang, S. Jeong, F. La Mantia, L.-F. Cui, and Y. Cui. 2009. "Highly Conductive Paper for Energy-Storage Devices." *Proceedings of the National Academy of Sciences* 106: 21490.

Hu, W., R. Chen, W. Xie, L. Zou, N. Qin, and D. Bao. 2014. "$CoNi_2S_4$ Nanosheet Arrays Supported on Nickel Foams with Ultrahigh Capacitance for Aqueous Asymmetric Supercapacitor Applications." *ACS Applied Materials & Interfaces* 6: 19318.

Huang, Y., T. Shi, S. Jiang, S. Cheng, X. Tao, Y. Zhong, G. Liao, and Z. Tang. 2016. "Enhanced Cycling Stability of $NiCo_2S_4$@NiO Core-shell Nanowire Arrays for All-Solid-State Asymmetric Supercapacitors." *Scientific Reports* 6: 38620.

Jiang, J., Y. Li, J. Liu, X. Huang, C. Yuan, and X. W. Lou. 2012. "Recent Advances in Metal Oxide-based Electrode Architecture Design for Electrochemical Energy Storage." *Advanced Materials* 24: 5166.

Justin, A. S., P. Vickraman, and B. J. Reddy. 2018. "Synthesis and Characterization of High Porous Carbon Sphere@nickel Oxide Core-shell Nanocomposite for Supercapacitor Applications." *Journal of Electroanalytical Chemistry* 823: 342.

Khani, H., and D. O. Wipf. 2017. "Iron Oxide Nanosheets and Pulse-Electrodeposited Ni–Co–S Nanoflake Arrays for High-Performance Charge Storage." *ACS Applied Materials & Interfaces* 9: 6967.

Lamiel, C., D. R. Kumar, and J.-J. Shim. 2017. "Microwave-Assisted Binder-Free Synthesis of 3D Ni- Co-Mn Oxide Nanoflakes@Ni

Foam Electrode for Supercapacitor Applications." *Chemical Engineering Journal* 316: 1091.

Lamiel, C., V. H. Nguyen, M. Baynosa, D. C. Huynh, and J. J. Shim. 2016. "Hierarchical Mesoporous Carbon Sphere@nickel Cobalt Sulfide Core–Shell Structures and Their Electrochemical Performance." *Journal of Electroanalytical Chemistry* 771: 106.

Li, Y., L. Cao, L. Qiao, M. Zhou, Y. Yang, P. Xiao, and Y. Zhang. 2014. "Ni–Co Sulfide Nanowires on Nickel Foam with Ultrahigh Capacitance for Asymmetric Supercapacitors." *Journal of Materials Chemistry A* 2: 6540.

Lin, J. Y., S. Y. Tai, and S. W. Chou. 2014. "Bifunctional One-Dimensional Hierarchical Nanostructures Composed of Cobalt Sulfide Nanoclusters on Carbon Nanotubes Backbone for Dye-Sensitized Solar Cells and Supercapacitors." *The Journal of Physical Chemistry C* 118: 823.

Lokhande, C. D., D. P. Dubal, and O.S. Joo. 2011. "Metal Oxide Thin Film Based Supercapacitors." *Current Applied Physics* 11: 255.

Manaf, N. S. A., M. S. A. Bistamam, and M. A. Azam. 2013. "Development of High Performance Electrochemical Capacitor: A Systematic Review of Electrode Fabrication Technique Based on Different Carbon Materials." *ECS Journal of Solid State Science and Technology* 2: M3101.

Meng, X., Q. Chang, C. Xue, J. Yang, and S. Hu. 2017. "Full-colour Carbon Dots: From Energy-efficient Synthesis to Concentration-dependent Photoluminescence Properties." *Chemical Communications* 53: 3074.

Mi, L., W. Wei, S. Huang, S. Cui, W. Zhang, H. Hou, and W. Chen. 2015. "A Nest-like Ni@$Ni_{1.4}Co_{1.6}S_2$ Electrode for Flexible High-performance Rolling Supercapacitor Device Design." *Journal of Materials Chemistry A* 3: 20973.

Mohamed, S. G., S. Y. Attia, and H. H. Hassan. 2017. "Spinel-structured $FeCo_2O_4$ Mesoporous Nanosheets as Efficient Electrode for Supercapacitor Applications." *Microporous and Mesoporous Materials* 251: 26.

Nguyen, V. H., C. Lamiel, D. Kharismadewi, V. C. Tran, and J.-J. Shim. 2015. "Covalently Bonded Reduced Graphene Oxide/polyaniline Composite for Electrochemical Sensors and Capacitors." *Journal of Electroanalytical Chemistry* 758: 148.

Nguyen, V. H., C. Lamiel, and J.-J. Shim. 2015. "Hierarchical Mesoporous Graphene@Ni-Co-S Arrays on Nickel Foam for High-performance Supercapacitors." *Electrochimica Acta* 161: 351.

Peng, T., H. Yi, P. Sun, Y. Jing, R. Wang, H. Wang, and X. Wang. 2016. "*In Situ* Growth of Binder-free CNTs@Ni–Co–S Nanosheets Core/shell Hybrids on Ni Mesh for High Energy Density Asymmetric Supercapacitors." *Journal of Materials Chemistry A* 4: 8888.

Pu, J., Z. Wang, K. Wu, N. Yu, and E. Sheng. 2014. "Co_9S_8 Nanotube Arrays Supported on Nickel Foam for High-performance Supercapacitor." *Physical Chemistry Chemical Physics* 16: 785.

Shown, I., A. Ganguly, L.-C. Chen, and K-H. Chen. 2014. "Conducting Polymer-Based Flexible Supercapacitor." *Energy Science & Engineering* 3: 2.

Snook, G. A., P. Kao, and A. S. Best. 2011. "Conducting-Polymer-Based Supercapacitor Devices and Electrodes." *Journal of Power Sources* 196: 1.

Sun, H., L. Mei, J. Liang, Z. Zhao, C. Lee, H. Fei, M. Ding, et al. 2017. "Three-Dimensional Holey-Graphene/Niobia Composite Architectures for Ultrahigh-rate Energy Storage." *Science* 356: 599.

Thommes, M., K. Kaneko, A. V. Neimark, J. P. Olivier, F. Rodriguez-Reinoso, J. Rouquerol, and K. S. Sing. 2015. "Physisorption of Gases, with Special Reference to the Evaluation of Surface Area and Pore Size Distribution." *Pure and Applied Chemistry* 87: 1051.

Wang, G., L. Zhang, and J. Zhang. 2012. "A Review of Electrode Materials for Electrochemical Supercapacitors." *Chemical Society Reviews* 41: 797.

Wang, H., C. M. B. Holt, Z. Li, X. Tan, B. S. Amirkhiz, Z. Xu, B. C. Olsen, T. Stephenson, and D. Mitlin. 2012. "Graphene-Nickel Cobaltite Nanocomposite Asymmetrical Supercapacitor with Commercial Level Mass Loading." *Nano Research* 5: 605.

Wang, X., X. Xia, L. G. Beka, W. Liu, and X. Li. 2016. "*In Situ* Growth of Urchin-like $NiCo_2S_4$ Hexagonal Pyramid Microstructures on 3D Graphene Nickel Foam for Enhanced Performance of Supercapacitors." *RSC Advances* 6: 9446.

Wei, C., Q. Ru, X. Kang, H. Hou, C. Cheng, and D. Zhang. 2018a. "Self-template Synthesis of Double Shelled ZnS-NiS1.97 Hollow Spheres for Electrochemical Energy Storage." *Applied Surface Science* 435: 993.

Wei, C., N. Zhan, J. Tao, S. Pang, L. Zhang, C. Cheng, and D. Zhang. 2018b. "Synthesis of Hierarchically Porous NiCo2S4 Core-shell Hollow Spheres via Self-template Route for High Performance Supercapacitors." *Applied Surface Science* 453: 288.

Wei, C., R. Zhang, X. Zheng, Q. Ru, Q. Chen, C. Cui, G. Li, and D. Zhang. 2018c. "Hierarchical Porous NiCo2O4/CeO2 Hybrid Materials for High Performance Supercapacitors." *Inorganic Chemistry Frontiers* 5: 3126.

Wen, Y., S. Peng, Z. Wang, J. Hao, T. Qin, S. Lu, J. Zhang, D. He, X. Fan, and G. Cao. 2017. "Facile Synthesis of Ultrathin $NiCo_2S_4$ Nano-Petals Inspired by Blooming Buds for High-Performance Supercapacitors." *Journal of Materials Chemistry A* 5: 7144.

Wu, L., Y. Wu, H. Wei, Y. Shi, and C. Hu. 2004. "Synthesis and Characteristics of NiO Nanowire by a Solution Method." *Materials Letters* 58: 2700.

Wu, Z., and X. B. Zhang. 2017. "Design and Preparation of Electrode Materials for Supercapacitors with High Specific Capacitance." *Acta Physico-Chimica Sinica* 33: 305.

Xiao, J., L. Wan, S. Yang, F. Xiao, and S. Wang. 2014. "Design Hierarchical Electrodes with Highly Conductive $NiCo_2S_4$ Nanotube Arrays Grown on Carbon Fiber Paper for High-Performance Pseudocapacitors." *Nano Letters* 14: 831.

Yan, M., Y. Yao, J. Wen, L. Long, M. Kong, G. Zhang, X. Liao, G. Yin, and Z. Huang. 2016. "Construction of a Hierarchical $NiCo_2S_4$@PPy Core–Shell Heterostructure Nanotube Array on Ni Foam for a High-Performance Asymmetric Supercapacitor." *ACS Applied Materials & Interfaces* 8: 24525.

Yang, J., C. Yu, X. Fan, S. Liang, S. Li, H. Huang, Z. Ling, C. Hao, and J. Qiu. 2016. "Electroactive Edge Site-Enriched Nickel–Cobalt Sulfide into Graphene Frameworks for High-Performance Asymmetric Supercapacitors." *Energy & Environmental Science* 9: 1299.

Yang, Z., C. Y. Chen, and H. C. Chang. 2011. "Supercapacitors Incorporating Hollow Cobalt Sulfide Hexagonal Nanosheets." *Journal of Power Sources* 196: 7874.

Yuan, C., H. B. Wu, Y. Xie, and X. W. Lou. 2014. "Mixed Transition-metal Oxides: Design, Synthesis, and Energy-Related Applications." *Angewandte Chemie International Edition* 53: 1488.

Zhai, Y., Y. Dou, D. Zhao, P. F. Fulvio, R. T. Mayes, and S. Dai. 2011. "Carbon Materials for Chemical Capacitive Energy Storage." *Advanced Materials* 23: 4828.

Zheng, Y., J. Xu, X. Yang, Y. Zhang, Y. Shang, and X. Hu. 2018. "Decoration NiCo2S4 Nanoflakes onto Ppy Nanotubes as Core-shell Heterostructure Material for High-performance Asymmetric Supercapacitor." *Chemical Engineering Journal 333*: 111.

Zhi, M., C. Xiang, J. Li, M. Li, and N. Wu. 2013. "Nanostructured Carbon–Metal Oxide Composite Electrodes for Supercapacitors: A Review." *Nanoscale* 5: 72.

Zhu, T., Z. Wang, S. Ding, J. S. Chen, and X. W. Lou. 2011. "Hierarchical Nickel Sulfide Hollow Spheres for High Performance Supercapacitors." *RSC Advances* 1: 397.

Zou, R., M. F. Yuen, L. Yu, J. Hu, C.-S. Lee, and W. Zhang. 2016. "Electrochemical Energy Storage Application and Degradation Analysis of Carbon-Coated Hierarchical $NiCo_2S_4$ Core-Shell Nanowire Arrays Grown Directly on Graphene/Nickel Foam." *Scientific Reports* 6: 20264.